



Fuel effects on NO_x emissions in partially premixed flames

Sayangdev Naha, Suresh K. Aggarwal *

Department of Mechanical and Industrial Engineering, University of Illinois at Chicago, 2039 ERF, 842 W. Taylor Street, Chicago, IL 60607, USA

Received 8 October 2003; received in revised form 23 April 2004; accepted 23 July 2004

Available online 11 September 2004

Abstract

The requirement to significantly reduce NO_x and particulate emissions while maintaining combustor performance is one of the main drivers for internal combustion engine research. Partially premixing and using fuel blends represent two promising approaches for reducing both the NO_x and the particulate emissions from flames. This paper reports on the results of a numerical investigation on the effects of using different fuels on NO_x emissions in counterflow partially premixed flames. The fuels investigated include methane, *n*-heptane, and their blends with hydrogen. The methane flame is computed using the GRI-3.0 mechanism, while the *n*-heptane flame is computed by combining the Held et al. oxidation mechanism with the Li and Williams NO_x mechanism. Results indicate that, with regard to their NO_x characteristics, partially premixed flames can be grouped into two distinct regimes, namely a double-flame regime, characterized by high levels of partial premixing and/or low strain rates (a_s) with two physically separated reaction zones, and a merged-flame regime, characterized by low levels of partial premixing and/or high a_s with nearly merged reaction zones. In the first regime, NO_x characteristics of both methane and *n*-heptane flames are strongly affected by changes in equivalence ratio (ϕ) and strain rate, while in the second regime, they exhibit a relatively weak dependence on ϕ and a_s . In addition, the *n*-heptane and methane flames established under identical conditions exhibit widely different NO_x emission behavior in the first regime but qualitatively similar behavior in the second regime. Major differences include (i) significantly higher NO level and NO_x emission index, (ii) much wider double-flame regime with regard to ϕ and a_s , (iii) dominance of the prompt mechanism over the thermal mechanism in the entire partially premixed regime, and (iv) noticeable reduction in NO_x emission with hydrogen addition for *n*-heptane flames compared to methane flames. These differences are attributable to the different fuel pyrolysis/oxidation chemistry of the two fuels, as the consumption of *n*-heptane occurs mainly through the C₂ path, while that of methane occurs mainly through the C₁ path. As a result, the amounts of C₂H₂ and, consequently, of CH radicals formed in *n*-heptane flames are significantly higher than those in methane flames and are responsible for the observed differences in NO_x characteristics of the two fuels. © 2004 The Combustion Institute. Published by Elsevier Inc. All rights reserved.

1. Introduction

Due to their immense practical relevance, NO_x emissions from various types of flames and com-

busion devices have been extensively investigated. Barlow and Carter [1] investigated experimentally the effects of temperature and mixture fraction on NO_x emission in H₂ jet flames. Hayhurst and Lawrence [2] reported an experimental investigation of NO_x emission in a fluidized bed combustor during burning of coal volatiles. Meunier and Carvalho [3] per-

* Corresponding author. Fax: +1-312-413-0447.
E-mail address: ska@uic.edu (S.K. Aggarwal).

formed experimental and numerical investigations on NO_x emissions from turbulent propane diffusion flames. Schlegel et al. [4] reported an experimental–numerical study on NO_x emissions from catalytically stabilized lean premixed methane–air flames. Poppe et al. [5] investigated control of NO_x emissions from confined methane–air premixed flames by imposing oscillations. Many researchers have also focused on the development of appropriate NO_x mechanisms for more detailed prediction and investigation of NO_x emissions from flames. These include the Li and Williams mechanism [6], the Warnatz and Klaus mechanism [7], the Leeds mechanism [8], and the mechanisms discussed by Miller and Bowman [9].

The NO_x reduction strategies based on using fuel diluents and fuel blends have also been examined. Roberts [10] performed an experimental investigation and observed reduction in both NO_x emission and soot formation using water injection. Rortveit et al. [11] investigated the effect of diluents such as NO₂, CO₂, and He on NO_x formation in H₂–air counterflow flames. Zhao et al. [12] studied the effect of OH radical on NO_x emission in methane–air diffusion flame with steam addition. It was noted that, although steam addition increased OH concentration, it reduced CH concentration, which led to subsequent reduction in NO_x emission.

Rortveit et al. [13] reported an experimental–numerical study of NO_x emissions in methane–hydrogen mixtures in a counterflow configuration. Al-Baghdadi [14] examined NO_x emissions in spark ignition engines using a hydrogen–ethanol mixture as fuel and observed a significant reduction (about 33%) in NO_x production when such a fuel mixture was used instead of gasoline. This was attributed to lower peak temperatures due to the higher heat of vaporization of alcohol. Choudhuri and Gollahali [15] studied the effect of using a hydrogen–hydrocarbon composite fuel in turbulent jet flames. Although increase of hydrogen content was shown to decrease CO and soot production, NO_x was found to increase.

Many recent studies dealing with NO_x emission have focused on partially premixed flames (PPFs) [16–23], motivated by the considerations that these flames may have superior pollutant emission characteristics and that the emissions from these flames may be minimized by appropriately modifying the level of partial premixing. Partially premixed flames are formed by mixing air (in less than stoichiometric amounts) into the fuel stream prior to the reaction zone, where additional air is available for complete combustion. These flames have also been studied due to their fundamental relevance to flame liftoff and stabilization, nonpremixed turbulent flames, and spray combustion. With regard to their NO_x emission characteristics, Gore and Zhan [16] performed a numeri-

cal investigation on the effect of partial premixing on NO_x production in methane–air PPFs and observed the existence of an optimum level of partial premixing that yielded the lowest NO_x emission index. Tanoff et al. [17] conducted a numerical–experimental study of counterflow methane–air PPFs and observed a drastic change in NO emission behavior as the flame changed from a merged-flame to a double-flame structure as the equivalence ratio (ϕ) was reduced below a certain threshold value. Ravikrishna and Laurendeau [18] also reported a numerical–experimental investigation on the effect of partial premixing on NO emission from counterflow methane–air flames. They compared the laser-induced fluorescence measurements of NO with predictions using the GRI-2.11 and GRI-3.0 mechanisms and noted that the GRI-3.0 mechanism overpredicted NO concentrations compared to the measurements and predictions based on the GRI-2.11 mechanism. A similar observation was made by Barlow et al. [19] in their numerical–experimental study of counterflow methane–air PPFs. Dupont and Williams [20] examined the dominant NO_x formation mechanisms in rich methane–air flames. Xue and Aggarwal [21] reported a numerical investigation of the NO_x emission characteristics of *n*-heptane counterflow PPFs. Their results also indicated an optimum level of partial premixing that yields the lowest NO_x emission index. In addition, it was observed that the NO formation rate in the nonpremixed zone is significantly higher than that in the rich premixed zone. This was attributed to the transport of acetylene from the rich premixed to the nonpremixed zone and the significantly higher concentrations of O and OH radicals in the latter zone.

The possibility of using fuel blends including fuel diluents to obtain superior pollutant emission characteristics seems to be a promising area of research. While previous investigations have focused on NO_x emissions in a variety of flames and configurations, issues pertaining to the use of fuel diluents and fuel blends for reducing NO_x emission have not been examined in detail. Moreover, to characterize the effects of fuel blends on NO_x, it is imperative to understand first how the NO_x characteristics are affected by the use of different fuels under identical conditions. Motivated by this consideration, the present study focused on the comparison of NO_x characteristics of methane/air and heptane/air PPFs. A detailed examination of the dominant pathways and concentration profiles of key radical species is used to explain the qualitative and quantitative differences in NO_x emission behavior of the two flames at various levels of partial premixing. In addition, the effect of fuel blends on NO_x emissions was examined by employing methane/hydrogen and heptane/hydrogen blends.

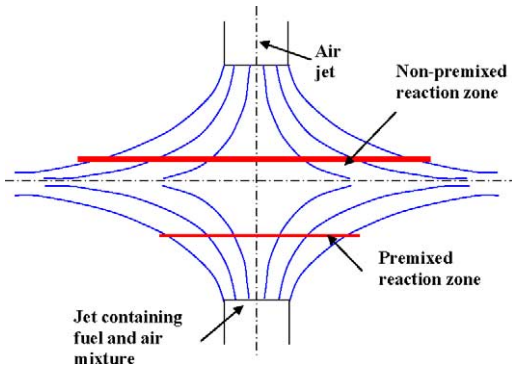


Fig. 1. Schematic of the counterflow flame configuration used in the present study.

2. Objective

The major objective of this study was to investigate the effects of using different fuels on NOx emissions in PPFs. To understand the NOx emission behavior of fuel blends, it is essential first to perform a detailed comparison of the NOx characteristics of pure fuels. For this purpose, the methane and *n*-heptane PPFs are simulated. Methane represents perhaps the most investigated gaseous fuel, while heptane is the most representative of liquid fuels. Moreover, detailed chemistry models for the oxidation of these two fuels have been extensively studied and validated. Thus, these two fuels provide a good starting point for studying the fuel effects on pollutant species.

Flame structures of heptane/air and methane/air partially premixed flames are compared to explain both the qualitative and the quantitative differences in the NOx emission behavior of the two flames. While previous studies have investigated the NOx emission characteristics of methane and *n*-heptane flames separately, they have not focused on the comparison of their flame structures and NOx emission behavior. In addition, the present study considers a complete partially premixed regime that includes both the double-flame and the merged-flame regimes and extends to the diffusion flame limit. It is important to consider these two regimes separately since the NOx characteristics of methane and *n*-heptane flames are significantly different in the two regimes. Previous investigations have not focused on this aspect. The present study also examines the issue of using fuel blends for reducing NOx emissions by employing methane/hydrogen and heptane/hydrogen fuel blends. A counterflow configuration as illustrated in Fig. 1 has been employed, since it facilitates detailed study of the dominant pathways associated with the various NOx mechanisms and the relative contributions of the premixed and nonpremixed reaction zones in NOx formation and destruction. Moreover, this con-

figuration makes it easier to separate the effects of stoichiometry and transport on the flame structure and NOx emissions.

3. Numerical model and boundary conditions

Simulations of partially premixed flames are performed using the OPPDIF code [24] in the Chemkin package [25]. The OPPDIF code is written in Fortran and used for computing the flow field in a counterflow configuration. The temperature of the fuel stream is taken as 400 K to ensure that the *n*-heptane fuel is in the gaseous phase. The air stream temperature is 300 K. The velocities of the fuel and oxidizer streams are chosen to conform to the global strain rate

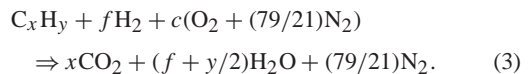
$$a_s = \frac{2|V_O|}{L} \left(1 + \frac{|V_F|\sqrt{\rho_F}}{|V_O|\sqrt{\rho_O}} \right) \quad (1)$$

and to satisfy the momentum balance

$$\rho_O V_O^2 = \rho_F V_F^2. \quad (2)$$

Using these two equations, the fuel and air stream velocities can be computed for a given value of the global strain rate a_s . The plug flow boundary conditions are used to specify the fuel and air stream velocities at the respective boundaries.

Boundary conditions for the species conservation equations require the specification of the species mole fractions at the two boundaries. For the simulation of flames burning pure fuels, the fuel side equivalence ratio provides the mole fractions of fuel, O₂, and N₂ species at the fuel nozzle, while the assumption of standard air composition provides the mole fractions of O₂ and N₂ at the air nozzle. For the simulations of flames burning fuel blends, we consider a blend containing 1 mole of hydrocarbon (C_xH_y) fuel and *f* mole (*f* being the molar ratio of H₂ to C_xH_y in the blend) of H₂. For PPFs, the fuel stream contains a mixture of fuel blend and air according to a specified equivalence ratio (ϕ). The mole fractions of various species at the fuel boundary are then computed using the following stoichiometric equation:



The mass balance yields $c = (x + f/2 + y/4)$. For a given ϕ , c on the right-hand side is replaced by $(x + f/2 + y/4)/\phi$. Then the mole fractions of C_xH_y, H₂, O₂, and N₂ at the fuel stream boundary can be obtained as

$$X(C_xH_y) = 84\phi/N,$$

$$X(H_2) = 84f\phi/N,$$

$$X(O_2) = 21(4x + y + 2f)/N,$$

and

$$X(N_2) = 79(4x + y + 2f)/N,$$

where the total number of moles, N , is given by

$$N = 400x + 100y + 200f + 84\phi + 84f\phi.$$

It is important to note that for the pure hydrocarbon fuel case, $f = 0$, while for nonpremixed flames, the fuel stream does not contain any air ($c = 0$).

The n -heptane oxidation chemistry is modeled by using the Held et al. mechanism [26]. It is combined with the NO_x chemistry model developed by Li and Williams [6], resulting in a full mechanism consisting of 54 species and 327 elementary reactions. The methane–air partially premixed flame is computed using the GRI-Mech 3.0 mechanism [27]. For both the methane and the n -heptane flames, the transport properties are computed using the mixture–average transport model. The transport properties for n -heptane flames were provided by Held et al. [26].

4. Results and discussion

4.1. Validation of reaction mechanisms

Both the methane and the n -heptane reaction mechanisms used in the present study have been previously validated for different configurations. The GRI-Mech 3.0 mechanism [27] and its earlier versions have been validated by many researchers using a variety of configurations. Sung et al. [28] validated the GRI-Mech 1.2 mechanism using experimental data for perfectly stirred reactors, autoignition and shock tube ignition delay times, ignition–extinction limits in counterflowing systems, and laminar flame propagation speeds. More recent studies reported by Xue et al. [22] and Barlow et al. [19] provide validation of the GRI-Mech 2.11 and 3.0 mechanisms for methane–air partially premixed flames in a counterflow geometry. Similarly the n -heptane mechanism used in the present study has been validated by Held et al. [26] using measurements in flow reactor, shock tube, stirred reactor, and freely propagating laminar flames. Another validation using a perfectly stirred reactor has been reported by Montgomery et al. [29]. Xue and Aggarwal [21] have provided additional validation of the mechanism for the simulation of premixed and nonpremixed heptane/air flames using measurements of Davis and Law [30] and Seiser et al. [31], respectively.

The NO_x mechanisms used in the present study have also been validated in previous investigations. Li and Williams [6] used the same NO_x mechanism to examine the effects of various diluents on NO_x

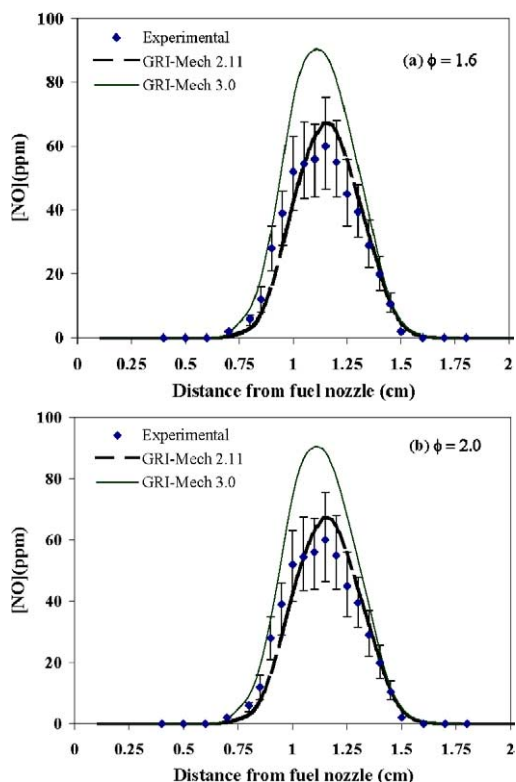


Fig. 2. Comparison of simulated NO mole fraction profile with experimental data from Ravikrishna and Laurendeau [18] for a methane/air PPF established at $a_s = 20 \text{ s}^{-1}$ and $\phi = 1.6$ (a) and $\phi = 2.0$ (b).

emissions in methane–air PPFs and reported excellent agreement between the measured and the predicted NO_x profiles. The validity of using this mechanism for NO_x emissions in n -heptane flames has been reported by Xue and Aggarwal [21]. The NO_x mechanisms used in GRI-Mech 2.11 and 3.0 have been evaluated by Ravikrishna and Laurendeau [18] and Barlow et al. [19], who compared the measured and predicted NO concentration profiles in methane–air PPFs. While both mechanisms provided good qualitative agreement with measurements, the GRI-Mech 3.0 overpredicted NO concentrations compared to the measurements and predictions based on the GRI-Mech 2.11. In the context of these two mechanisms, it is important to mention that while the nonpremixed flame structures predicted using these mechanisms are essentially the same, the differences between the mechanisms become more significant for PPFs. This aspect has been examined further in [22].

In the present study, we report two additional validations of the reaction mechanisms. For the first validation, we compare the predicted NO concentration profiles based on the GRI-Mech 2.11 and 3.0 mechanisms with measurements reported in [28]. Fig. 2

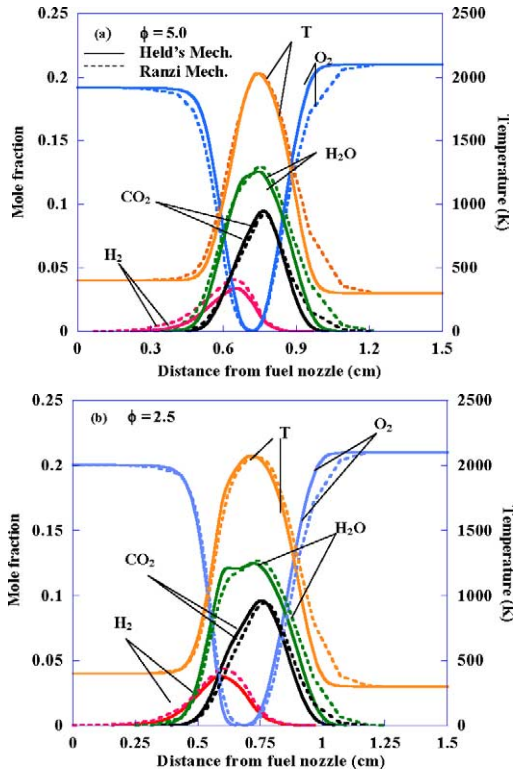


Fig. 3. Comparison of temperature and major species mole fraction profiles computed using the Held et al. mechanism and a more comprehensive mechanism for *n*-heptane/air PPFs established at $a_s = 100 \text{ s}^{-1}$ and $\phi = 5.0$ (a) and $\phi = 2.5$ (b).

presents this comparison for methane–air PPFs established at a global strain rate of $a_s = 20 \text{ s}^{-1}$ and fuel side equivalence ratios of $\phi = 1.6$ and 2.0. For both of these cases, the NO mole fraction profiles based on the GRI-Mech 2.11 are in good agreement with measurements, while those based on the GRI-Mech 3.0 are overpredicted. These results are consistent with those reported by Ravikrishna and Laurendeau [18] and Barlow et al. [19]. In both of these studies, the GRI-Mech 3.0 overpredicted NO levels compared to those based on the GRI-Mech 2.11 and the measurements.

The second validation pertains to the Held et al. [26] mechanism for predicting the *n*-heptane partially premixed flame structure. Here we compare numerical results based on the Held et al. mechanism with those based on a more comprehensive mechanism reported by Ranzi et al. [32]. Fig. 3 shows this comparison with regard to the temperature and major species profiles for heptane/air partially premixed flames established at $\phi = 5.0$ and 2.5 with a global strain rate of $a_s = 100 \text{ s}^{-1}$. The distance between the two nozzles is 1.5 cm and the fuel and air streams are introduced

at temperatures of 400 and 300 K, respectively. For both mechanisms, results for $\phi = 5.0$ indicate a partially premixed flame in the merged-flame regime, in which the two reaction zones are merged, and results for $\phi = 2.5$ indicate a partially premixed structure in the double-flame regime, characterized by the presence of a rich premixed reaction zone on the fuel side and a nonpremixed reaction zone on the oxidizer side. Overall, there is an excellent agreement between the two simulations, providing further validation of the Held et al. mechanism.

4.2. Structure and NO_x characteristics of methane and *n*-heptane PPFs

The grid independence of the computed results was achieved by controlling the values of the GRAD and CURV parameters and using adaptive regridding to resolve the structures of both the premixed and the nonpremixed reaction zones. The computed results were found to be essentially grid independent when the number of grid points was changed from 130 to 250. The results presented in this paper employed 160 grid points.

Having provided grid independence and validation of the reaction mechanisms for both the oxidation and the NO_x chemistry of the two fuels, we now focus on the comparison of the NO_x characteristics of methane and *n*-heptane partial premixed flames. In this context, partially premixed combustion can be classified into two distinct regimes, namely a double-flame regime and a merged-flame regime. In the first regime, a partially premixed flame contains two distinct or physically separated reaction zones, while in the second regime, the two reaction zones are nearly merged. For counterflow flames at atmospheric pressure, these two regimes can be represented with regard to ϕ and a_s . The double-flame regime is characterized by relatively low ϕ (high levels of partial premixing) and low a_s values. As ϕ (or a_s) is increased at fixed a_s (or ϕ), the two reaction zones move closer to each other and eventually merge, indicating a transition to the merged-flame regime. A detailed discussion on the effects of ϕ and a_s on the transition has been provided in a previous investigation [33]. As discussed in [33], increasing ϕ at constant a_s essentially affects the rich premixed zone, which moves away from the fuel nozzle or toward the nonpremixed zone, while increasing a_s at constant ϕ causes the nonpremixed zone to move toward the rich premixed zone. The flame structure and interactions between the reaction zones are different in the two regimes. As a result, the NO_x characteristics of methane and *n*-heptane flames are found to be significantly different in the two regimes. Consequently, it is relevant to examine each regime separately.

4.3. Comparison of NO_x characteristics in the double-flame regime

A direct quantitative comparison of the NO_x characteristics of methane and *n*-heptane PPFs under identical conditions is somewhat limited due to their significantly different double-flame regimes. For counterflow flames at atmospheric pressure, this regime is represented by a range of ϕ and a_s for which a PPF contains two distinct or physically separated reaction zones. As ϕ is increased, the range of a_s for this regime becomes narrower, with a similar effect occurring when a_s is increased. Previous experimental and numerical studies [6,17,22,23] have observed that the double-flame regime for counterflow methane–air flames is approximately given by $1.4 < \phi < 2.0$ and $20 < a_s < 50 \text{ s}^{-1}$. As ϕ is increased above 2.0 and/or a_s is increased above 50 s^{-1} , the distance between the two reaction zones decreases, and the flame structure approaches the merged-flame regime. For heptane–air counterflow flames, previous studies [21,34] indicate that the corresponding double-flame regime is given by $1.5 < \phi < 3.5$ and $20 < a_s < 120 \text{ s}^{-1}$. A comparison of the double-flame regimes for the two fuels thus indicates a rather narrow range of ϕ and a_s in which both the methane and the *n*-heptane flames exhibit a double-flame structure and can be compared with regard to their NO_x characteristics. Consequently, we select two cases, with regard to ϕ and a_s , to compare the flame structure and NO_x characteristics of methane and *n*-heptane PPFs.

Figs. 4 and 5 present a comparison of the structures of methane/air and *n*-heptane/air PPFs, both established at $\phi = 1.6$, and $a_s = 40 \text{ s}^{-1}$. The fuel and air stream temperatures are 400 and 300 K, respectively, and the distance between the two nozzles is 2 cm. Fig. 4 presents the temperature and major species mole fraction profiles, while Fig. 5 shows the profiles of temperature and the mole fractions of some species relevant to NO formation. The global flame structure for the two fuels is similar in the sense that for both fuels the flame contains two distinct reaction zones, namely a rich premixed reaction zone on the fuel side and a nonpremixed reaction zone on the oxidizer side. The premixed reaction zone is characterized by the fuel-rich oxidation chemistry that involves the pyrolysis/consumption of fuel, the production of “intermediate fuel” species (C₂H₂, CO, and H₂), and to a lesser extent production of CO₂ and H₂O. The intermediate fuel species are transported to the nonpremixed reaction zone, where they are oxidized to form CO₂ and H₂O. Thus, the nonpremixed zone is characterized by the oxidation of these intermediate fuel species.

Apart from this global similarity, the structures of methane and *n*-heptane flames exhibit significant

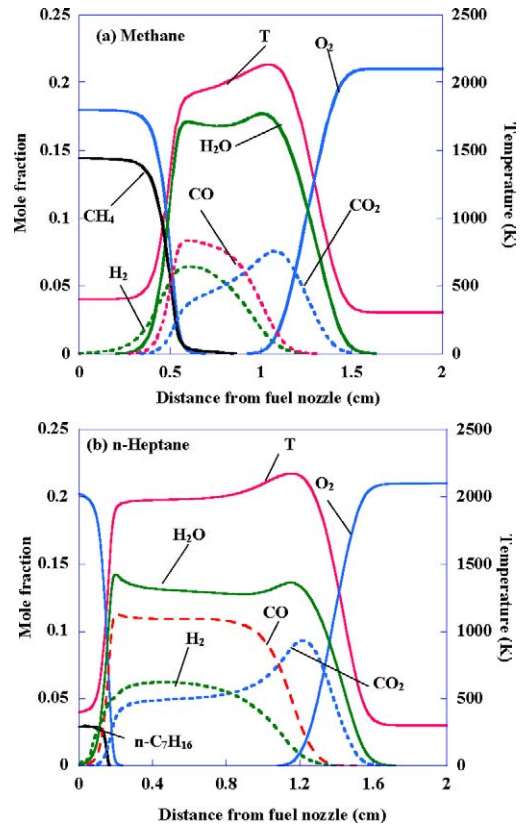


Fig. 4. Temperature and major species mole fraction profiles for (a) methane/air and (b) *n*-heptane/air PPFs established at $a_s = 40 \text{ s}^{-1}$ and $\phi = 1.6$.

differences, although they are established under identical conditions. One important difference pertains to their flame topology, in particular the location of the premixed reaction zone and the distance between the two reaction zones. The premixed reaction zones for the methane and *n*-heptane flames are located at 0.55 and 0.2 cm, respectively, while the two corresponding nonpremixed reaction zones are located at $x \approx 1.2$. Thus, the separation distances between the two reaction zones are 0.65 and 1.0 cm, respectively, for the two cases. This difference can be attributed to the fuel-rich or low-temperature oxidation chemistry of the two fuels. The pyrolysis/oxidation chemistry of methane is known to be slow compared to that of higher hydrocarbon fuels (*n*-heptane in the present case), and, consequently, the rich premixed zone for the methane flame is located farther downstream from the fuel nozzle than that for the *n*-heptane flame. The evidence for the slower pyrolysis/oxidation chemistry of methane is provided by its ignition characteristics, i.e., the minimum ignition temperature and the ignition delay time. As reported in [35,36], the autoignition temperatures of methane/air and *n*-heptane/air

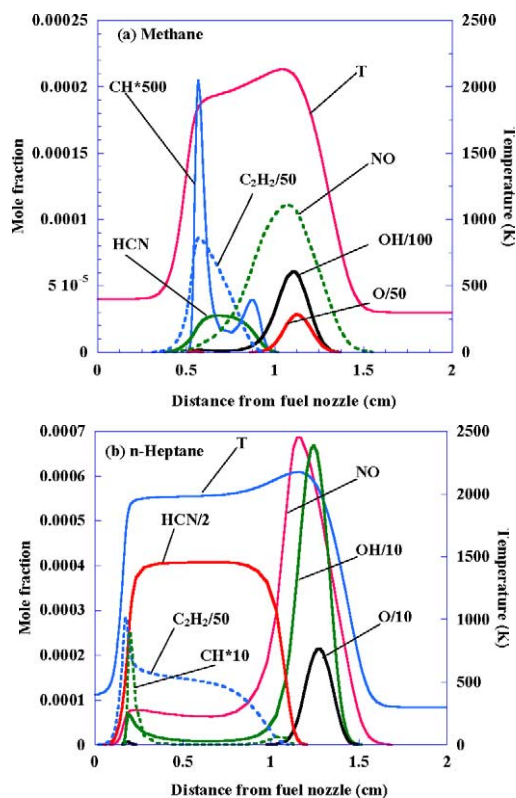


Fig. 5. Temperature and NO and intermediate species mole fraction profiles for (a) methane/air and (b) *n*-heptane/air PPFs discussed in the context of Fig. 4.

mixtures at 1 atm are 810 and 477 K, respectively. In addition, the shock tube data reported by Horning et al. [37] and Hidaka et al. [38] indicate that the ignition delay times for methane/air and *n*-heptane/air mixtures under similar conditions are 0.8 and 0.16 ms, respectively. Due to the differences in ignition characteristics, which are related to the fuel-rich low-temperature oxidation chemistry, the premixed reaction zone in methane flame is located farther downstream (from the fuel nozzle) than that in *n*-heptane flame, and this leads to a greater separation distance between the reaction zones in *n*-heptane flame. It is also worth mentioning that the Held et al. mechanism, being a high-temperature mechanism, does not include the low-temperature chemistry. However, the predicted H_2O_2 and OH profiles (not shown) indicated that the H_2O_2 mole fraction in the premixed reaction zone was significantly higher than that in the nonpremixed zone, while the OH mole fraction was significantly higher in the premixed reaction zone than in the nonpremixed zone. This implies that the intermediate-temperature chemistry involving fuel + HO_2 producing H_2O_2 , and H_2O_2 decomposing to give OH radicals, plays a role in determining the lo-

cation of the premixed reaction zone of *n*-heptane PPFs.

A major difference between the two flames, in the context of their NO_x characteristics, is exhibited by the C_2H_2 and CH concentration profiles presented in Fig. 5. As discussed below, the difference in the NO_x characteristics of methane and *n*-heptane PPFs can be attributed to their flame structures and especially to the C_2H_2 and CH profiles. Important observations with regard to these differences include the following:

- (1) The peak C_2H_2 value, which occurs in the premixed zone, is about four times higher for *n*-heptane flame than for methane flame (cf. Fig. 5). A rate of production analysis (ROPA) was performed to characterize the fuel consumption behavior in the two flames. It was observed that, for the present case, 60% of methane is consumed through the C_1 path, while 40% is consumed through the C_2 path. In contrast, for *n*-heptane flame, more than 90% of the fuel is consumed through the C_2 path, with the remaining being consumed through the C_1 path. This explains why the C_2H_2 concentration is much higher in *n*-heptane flame than in methane flame. A similar difference in C_2H_2 concentrations is observed for other cases investigated in the present study. There are two points worth mentioning here. First, as discussed in [21], the C_1 – C_2 characterization has extended to heptane–air chemistry, since C_3 – C_6 species are decomposed mainly to C_3H_5 , which is converted to C_4H_6 , which is then converted to vinyl, acetylene, and $\text{C}_2\text{H}_3\text{HCO}$. Second, the Held et al. mechanism has been shown to overpredict C_2H_2 concentrations [21, 37], and this would lead to an overprediction of prompt NO for *n*-heptane flames.
- (2) Due to the high acetylene concentration in *n*-heptane flames, only a fraction of acetylene is consumed in the premixed reaction zone, producing CH in this zone; as indicated in Fig. 5b, the CH peak in the premixed zone coincides with the sharp drop in C_2H_2 mole fraction.¹ The remaining C_2H_2 is transported to the nonpremixed reaction zone, producing additional CH there. Consequently, the CH profile exhibits two peaks, one in the premixed zone and the other in the nonpremixed zone. However, most of the prompt NO is produced in the nonpremixed zone, even though the CH peak in the premixed zone is

¹ Previous investigations of partially premixed flames [6,21] have established that C_2H_2 is the major source of CH in these flames. This was further confirmed by performing a rate of production analysis in the present study.

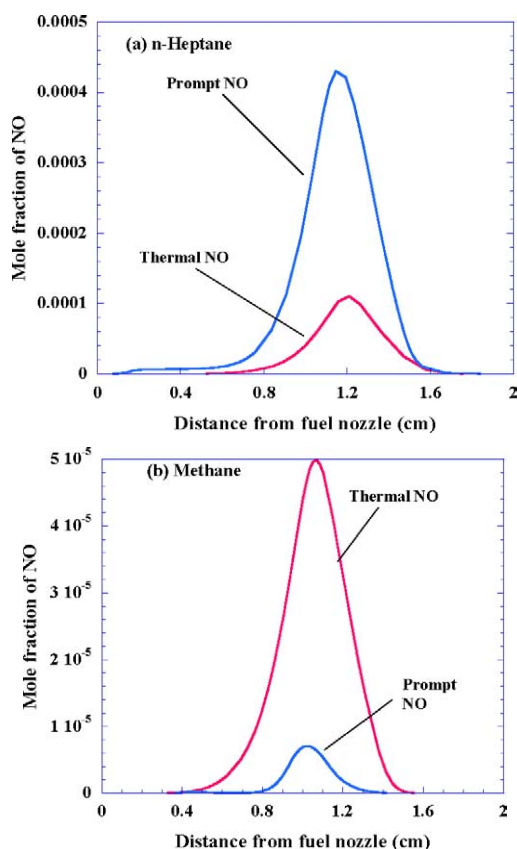


Fig. 6. Mole fraction profiles of the prompt and thermal NO for (a) *n*-heptane/air and (b) methane/air PPFs discussed in the context of Fig. 4.

much higher than that in the nonpremixed zone. This is shown clearly in Fig. 6a, which presents the mole fraction profiles of prompt and thermal NO, and it can be attributed to the paucity of O and OH radicals in the premixed reaction zone. While the presence of CH radicals immediately leads to the formation of HCN through the reaction $\text{CH} + \text{N}_2 \leftrightarrow \text{HCN} + \text{N}$, the subsequent conversion of HCN to NO occurs mainly in the nonpremixed zone due to the availability of O and OH radicals in that zone. This is clearly indicated by the mole fraction profiles of CH, HCN, O, and OH species in Fig. 5b.

- (3) In both *n*-heptane and methane flames, most of the NO is produced in the nonpremixed zone (cf. Fig. 6). However, while most of the NO is produced through the prompt mechanism in *n*-heptane flame, it is produced mainly through the thermal mechanism in methane flame. This represents an important difference with regard to the NO_x characteristics of the two flames and is directly related to the significantly higher amount

of C₂H₂ produced in *n*-heptane flame. As discussed above, for *n*-heptane flame, a significantly higher amount of C₂H₂ is produced in the pre-mixed reaction zone and, consequently, transported to the nonpremixed zone. This leads to a much higher concentration of CH and, consequently, much higher concentrations of HCN and prompt NO in the nonpremixed zone of *n*-heptane flame. This is clearly indicated by the comparison of the two flames in Figs. 5 and 6. Similar behavior was observed for the other cases investigated in the double-flame regime.

- (4) The ROPA analysis [39] indicated that while acetylene is the major source of CH in both the *n*-heptane and the methane flames, the amount of CH produced for a given amount of acetylene is much smaller in methane flame than in heptane flame. This is directly related to the oxidation chemistries of the two fuels² and further explains why, in the double-flame regime, most of the NO is due to the thermal mechanism in methane flames and to the prompt mechanism in *n*-heptane flames.
- (5) Another important observation from Figs. 5 and 6 is the much higher NO level in *n*-heptane flame compared to that in methane flame. For the case presented in Figs. 5 and 6, the peak NO value in *n*-heptane flame is about seven times higher than that in methane flame and is mainly due to the much higher level of prompt NO in *n*-heptane flame. As indicated in Fig. 6, the peak values of prompt and thermal NO in *n*-heptane flame are, respectively, about six and two times higher than those in methane flame. The higher prompt NO in *n*-heptane flame is due to the significantly larger amount of acetylene transported to the nonpremixed reaction zone, while the higher thermal NO is due to the higher temperature and higher concentrations of O and OH radicals in the nonpremixed zone. The peak temperatures for the *n*-heptane and methane flames presented in Figs. 5 and 6 are ≈ 2180 and 2130 K, while the peak O mole fractions are ≈ 0.0022 and 0.00143, respectively. It is important to note that the adiabatic

² The pathway analysis indicated that a significantly higher (about two times) amount of C₂H₂ is converted to CH₂ for *n*-heptane flames than for methane flames. More importantly, the amount of CH₂ converted to CH is an order of magnitude higher for *n*-heptane flames than for methane flames. This is due to the fact that, for methane flames, most of the CH₂ is converted to CO through its reaction with O₂, while for *n*-heptane flames, the conversion to CO is relatively small.

flame temperatures for *n*-heptane and methane flames are 2484 and 2226 K, respectively.

- (6) In both methane and *n*-heptane flames, NO concentration in the rich premixed zone is negligible compared to that in the nonpremixed zone. This is due to the lower temperature and lower concentrations of O and OH radicals in the premixed zone. As discussed in [6,21], the presence of CH, OH, and O is essential for prompt NO and that of OH and O for thermal NO. Moreover, the paucity of OH and O radicals in the premixed zone makes the reburn mechanism more active, which further diminishes the formation of prompt NO in this zone. The participation of the reburn mechanism is more evident in *n*-heptane flame (cf. Fig. 5b), which shows a decrease in the NO mole fraction in the region between the two reaction zones. Important reaction pathways associated with the prompt, thermal, and reburn NO mechanisms in *n*-heptane flames have been discussed previously in [21]. As discussed in the cited study, the reburn mechanism involves the conversion of NO to HCN and HNCO, mainly through reactions $\text{NO} + \text{CH} \rightleftharpoons \text{HCN} + \text{O}$ and $\text{NO} + \text{CH}_2 \rightleftharpoons \text{HNCO} + \text{H}$.

Fig. 7 presents a comparison of the structures of methane/air and *n*-heptane/air PPFs for another set of identical conditions, with $\phi = 2.0$ and $a_s = 100 \text{ s}^{-1}$. The temperature and species profiles for *n*-heptane depict a partially premixed flame in the double-flame regime, i.e., containing two distinct reaction zones. However, the profiles for methane indicate a broadened flame in the merged-flame regime, as the two reaction zones are nearly merged. Similar to the case discussed in the context of Figs. 4–6, the NO level for this case is also significantly higher in *n*-heptane flame than in methane flame. In addition, for both fuels, the NO level in the rich premixed zone is negligible compared to that in the nonpremixed zone, which is also similar to the previous case. However, there is one notable difference between the two cases. In the previous case (cf. Fig. 6), the prompt mechanism was the major contributor to total NO for the *n*-heptane flame, while the thermal mechanism was the major contributor for the methane flame. However, for the case presented in Fig. 7, the prompt mechanism becomes the major contributor to total NO for both the *n*-heptane and the methane flames. This crossover from thermal NO to prompt NO occurs only for methane flames and represents an important difference between the NOx characteristics of the two fuels. As discussed in the next section, this is related to the transition from the double-flame to the merged-flame regime.

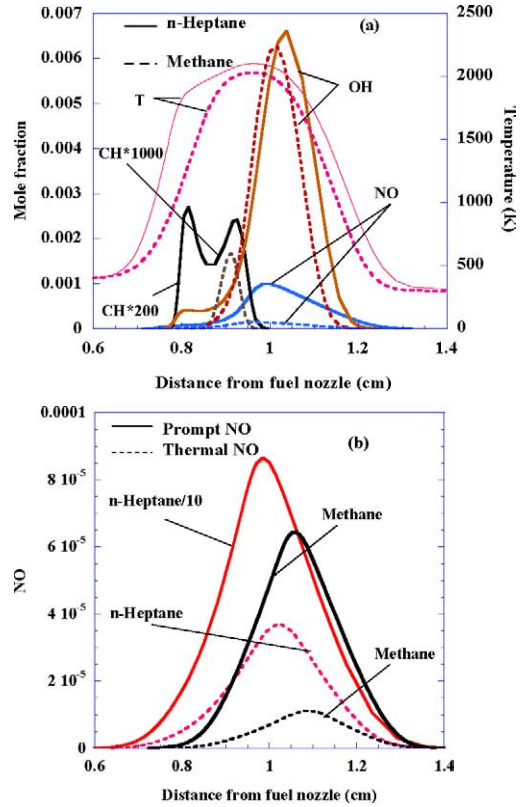


Fig. 7. Comparison of methane and *n*-heptane partially premixed flame structures for $a_s = 100 \text{ s}^{-1}$ and $\phi = 2$. Temperature and species mole fraction profiles are shown in (a); prompt and thermal NO profiles are shown in (b).

4.4. Comparison of NOx characteristics in the merged-flame regime

The double-flame regime discussed in the preceding section is characterized by relatively high levels of partial premixing and low strain rates. With increasing ϕ and/or a_s , the two reaction zones move closer and eventually merge, representing a transition to the merged-flame regime. Fig. 8 presents the profiles of temperature and some species relevant to NO formation for methane/air and *n*-heptane/air PPFs established at conditions corresponding to this regime. The global flame structures for the two fuels appear to be similar in this regime. Note, however, that the methane flame is established at $\phi = 1.8$ and $a_s = 40 \text{ s}^{-1}$, while the *n*-heptane flame is established at $\phi = 2.8$ and $a_s = 50 \text{ s}^{-1}$. Similar to the cases discussed for the double-flame regime, most of the NO is produced in the nonpremixed zone for both the flames, and the NO level in *n*-heptane flame is much higher than that in methane flame.

The major difference between the double-flame and the merged-flame regimes is due to the relative

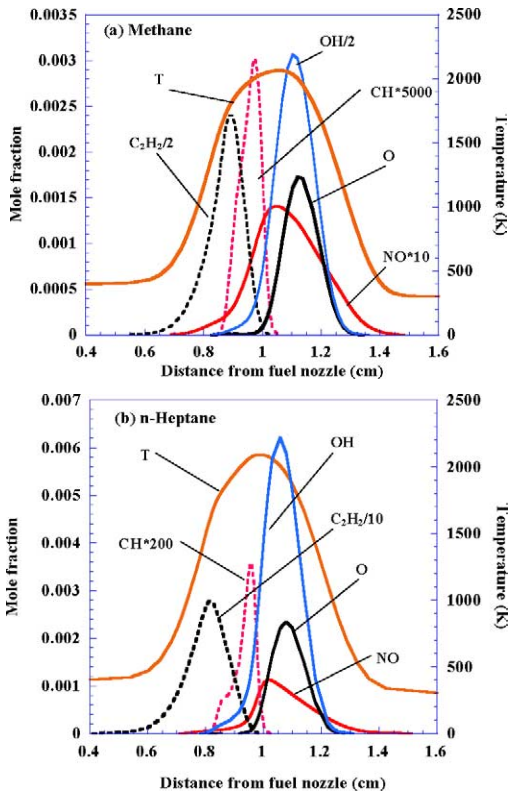


Fig. 8. Comparison of temperature and species mole fraction profiles for methane (a) and *n*-heptane (b) partially premixed flames in the merged-flame regime. For methane flame, $a_s = 50 \text{ s}^{-1}$ and $\phi = 2.0$; for *n*-heptane flame, $a_s = 50 \text{ s}^{-1}$ and $\phi = 2.8$.

contributions of the prompt and thermal mechanisms for the two fuels. This difference is clearly seen by comparing the thermal and prompt NO profiles for the two fuels in the double-flame and merged-flame regimes, presented in Figs. 6 and 9, respectively. In the double-flame regime depicted in Fig. 6, the prompt mechanism is the major contributor to total NO in *n*-heptane flames, while the thermal mechanism is the major contributor to total NO in methane flames. However, in the merged-flame regime depicted in Fig. 9, the prompt mechanism becomes the major contributor to total NO in both the *n*-heptane and the methane flames. Thus, for methane flames, there is a switch between the relative contributions of the thermal and prompt NO during the transition from the double-flame to the merged-flame regime. There is no such crossover, however, for *n*-heptane flames, as the prompt NO remains the major contributor to the total NO in the entire partially premixed regime. This represents an important difference in the NO_x characteristics of *n*-heptane and methane partially premixed flames and has not been reported by previous investigations.

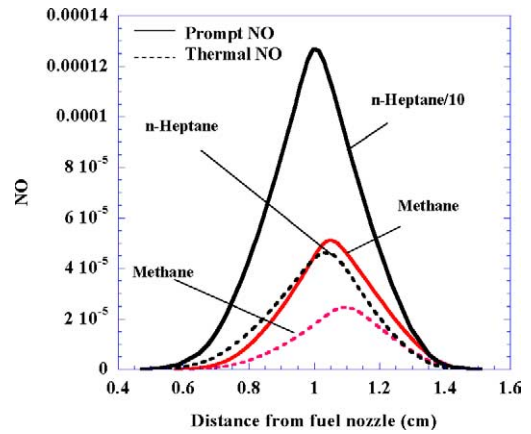


Fig. 9. Mole fraction profiles of the prompt and thermal NO in methane and *n*-heptane/air PPFs discussed in the context of Fig. 8.

Several additional simulations were performed to characterize the effects of ϕ and a_s on the relative contributions of the prompt and thermal mechanisms in the two reaction zones and to confirm the crossover observed for methane flames. The general observations with regard to the relative contributions of the prompt and thermal mechanisms and with regard to the crossover for methane flames were the same as those discussed in the preceding sections.

4.5. Comparison of NO_x characteristics with regard to NO_x emission index (EINO_x)

The global NO_x characteristics of methane and *n*-heptane PPFs can be compared by plotting the NO_x emission index as a function of fuel-rich equivalence ratio and global strain rate. The NO_x emission index is defined as

$$EINO_x = \frac{\int_0^L M_{NO_x} \dot{\omega}_{NO_x} dx}{-\int_0^L M_{fuel} \dot{\omega}_{fuel} dx} \quad (4)$$

Here, M represents the molecular weight, $\dot{\omega}$ is the net production/consumption rate, L is the distance between the nozzles, and x is the axial coordinate. The emission index is a global parameter that has been commonly used to characterize NO_x emission from different flames [6,16,21].

Fig. 10 presents the NO_x emission index as a function of ϕ for *n*-heptane and methane PPFs established at strain rates of $a_s = 50$ and 100 s^{-1} . There are two important observations from this figure. One, EINO_x is much higher for *n*-heptane flames than for methane flames. While their relative values depend upon ϕ and a_s , EINO_x for *n*-heptane flames is generally 5 to 10 times higher than that for methane flames. This is consistent with the results presented in the preceding

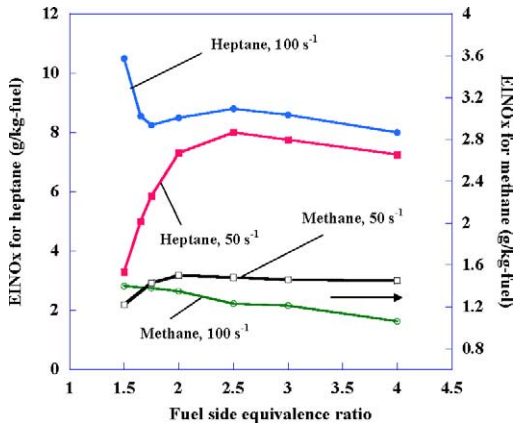


Fig. 10. NOx emission index plotted versus ϕ for methane and *n*-heptane PPFs established at $a_s = 50$ and 100 s^{-1} .

sections and can be attributed to the dominant pathways involving the C_1 and C_2 species, leading to a significantly higher amount of acetylene being produced in *n*-heptane flames. Two, with regard to the dependence of EINOx on ϕ in the double-flame and merged-flame regimes, in the double-flame regime, the EINOx exhibits strong dependence on ϕ , while in the merged-flame regime, the emission index has a weak dependence on ϕ , decreasing slowly to the diffusion flame limit as ϕ is increased.

As noted earlier, the ranges of ϕ and a_s for the double-flame regime are significantly different for the two fuels. For *n*-heptane flames, this regime is approximately given by $1.5 < \phi < 3.5$ and $20 < a_s < 120 \text{ s}^{-1}$, while for methane flames, it is given by $1.4 < \phi < 2.0$ and $20 < a_s < 50 \text{ s}^{-1}$. Moreover, as a_s (or ϕ) increases, the range of ϕ (or a_s) for the double-flame region becomes narrower for both fuels. For *n*-heptane flames at $a_s = 50 \text{ s}^{-1}$, this regime is given by $1.5 < \phi < 3.0$. In this regime, as indicated in Fig. 10, the EINOx first increases and then decreases with ϕ . In the merged-flame regime ($\phi > 3.0$), the EINOx decreases slowly with ϕ as it approaches the diffusion flame limit. A similar behavior is observed for methane flames at $a_s = 50 \text{ s}^{-1}$, except that the double-flame regime is narrower, given by $1.4 < \phi < 2.0$, and the EINOx is much lower than that for *n*-heptane flames. The EINOx values in the diffusion flame limit are 7.2 and 1.3, respectively, for *n*-heptane and methane flames. The above results are consistent with those reported by previous researchers. For *n*-heptane flames, a detailed discussion on the variation of EINOx with ϕ has been provided by Xue and Aggarwal [21]. As discussed in the cited study, for $a_s = 50 \text{ s}^{-1}$, the variation of EINOx with ϕ in the double-flame region is related to the interaction of the two reaction zones as the level of the partial premixed zone is reduced. For lower ϕ ($\phi = 1.5$), the

premixed reaction zone is located far from the non-premixed zone. Consequently, there is little transport of C_2H_2 from the premixed zone to the nonpremixed zone, and this reduces the prompt NO formation rate in the latter zone. This in turn decreases the total NO formation rate, since most of the NO in *n*-heptane flames formed due to the prompt mechanism. As ϕ is increased, interactions between the two reaction zones are enhanced due to the reduced separation distance between them and the transport of C_2H_2 to the nonpremixed zone becomes significant. This causes a significant increase in the prompt NO formation rate in the nonpremixed zone. The thermal NO formation rate in this zone is also enhanced due to the increased radical activity. Consequently, as ϕ is increased, the total NO formation rate increases, which leads to higher EINOx. This trend does not continue, however, since further increase in ϕ leads to a transition from the double-flame to the merged-flame regime, and EINOx then decreases slowly with ϕ . Our results with regard to the variation of EINOx with ϕ for methane PPFs are consistent with those reported in previous investigations [6,23,40]. The computed EINOx values in the present study agree well with those reported by Li and Williams [6]. For example, for a methane flame established at $\phi = 3.0$ and $a_s = 50 \text{ s}^{-1}$, the EINOx values in our simulation and in [6] are 1.46 and 1.4, respectively. There is also good qualitative agreement between our results and those reported by Blevins and Gore [23] and Nishioka et al. [40], although a quantitative comparison could not be done due to different parameters.

For the higher-strain case ($a_s = 100 \text{ s}^{-1}$), the double-flame regime for *n*-heptane flames is given by $1.5 < \phi < 2.5$, and in this range, the EINOx first decreases, reaching a minimum at $\phi \approx 1.75$, and then increases as ϕ is increased up to 2.5. For $\phi > 2.5$, which corresponds to the merged-flame region, the EINOx again decreases slowly to the diffusion flame value of 7.93 as ϕ is increased. For methane flames at $a_s = 100 \text{ s}^{-1}$, there is no double-flame region, and, consequently, the EINOx decreases slowly to the diffusion flame limit.

4.6. Effect of using fuel blends on NOx emissions

The second part of this paper focuses on the effect of adding hydrogen on the NOx characteristics of methane and *n*-heptane flames. For methane flames, we employed two different approaches to characterize the effect of hydrogen addition on NOx emission. In the first approach, which has been used previously by Rortveit et al. [13], the peak flame temperature for different CH_4-H_2 blends is kept constant by using nitrogen dilution. The objective is to validate our results by comparing them with those from the cited study

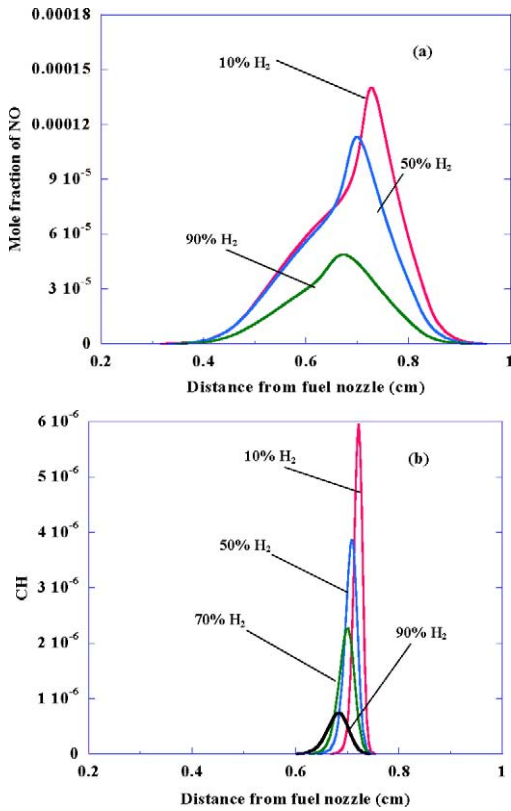


Fig. 11. NO (a) and CH (b) mole fraction profiles for nonpremixed flames established with different methane/hydrogen blends at a strain rate of 100 s^{-1} . Nitrogen dilution is used to maintain the peak flame temperature at 2040 K for all the cases.

and to eliminate the temperature effect on NO_x emission as the amount of hydrogen addition is increased. In the second approach, no nitrogen dilution is used, which allows us to characterize the effect of hydrogen addition on both the prompt and the thermal NO.

Fig. 11 presents the NO and CH mole fraction profiles for nonpremixed flames simulated using CH₄–H₂ blends with nitrogen dilution. The global strain rate is 100 s^{-1} and the distance between the nozzles is 1.27 cm. Results are presented for four different blends containing 0, 10, 50, and 90% H₂ by volume. For all four cases, the peak flame temperature was maintained at 2040 K using nitrogen dilution. Results for the 0% hydrogen case were indistinguishable from those for the 10% hydrogen case and are not shown in the figure. As indicated in Fig. 11a, as the H₂ concentration is increased, the amount of NO formed decreases in a monotonic manner. This is due to a reduction in prompt NO, since thermal NO remains essentially the same as the flame temperature is maintained constant. These results are consistent with those reported by Rortveit et al. [13]. Further insight

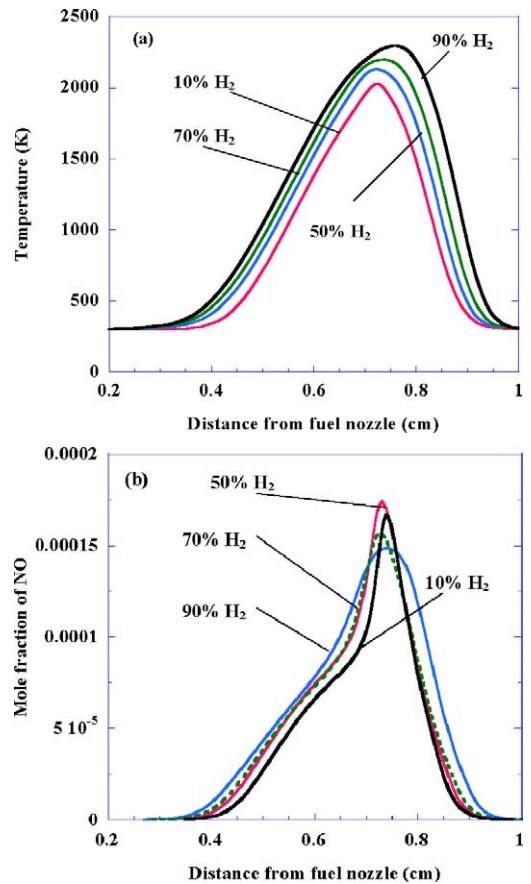


Fig. 12. Temperature (a) and NO mole fraction (b) profiles for nonpremixed flames established at $a_S = 100 \text{ s}^{-1}$, using different methane/hydrogen blends without nitrogen dilution.

into this behavior is provided by the CH profiles presented in Fig. 11b. As the amount of H₂ in the blend is increased, the CH concentration decreases, since the amount of methane in the fuel blend decreases, which in turn decreases the prompt NO. It is worth mentioning, however, that a relatively large amount of H₂ is needed to bring a noticeable reduction in NO_x emission. For example, addition of 10% H₂ by volume (1.4% by mass) has essentially no effect on the computed NO profile, while addition of 50% H₂ by volume (or 11.1% by mass) decreases the peak NO value by about 30%.

Fig. 12 presents the temperature and NO mole fraction profiles for nonpremixed flames using CH₄–H₂ blends without nitrogen dilution. Results are shown for four different blends containing 10, 50, 70, and 90% H₂ by volume, or 1.4, 11.1, 22.6, and 52.9% H₂ by mass. Results for the 0% H₂ were again indistinguishable from those for 10% H₂ and are not included in the figure. As expected, H₂ addition in the fuel blend increases the flame temperature (cf.

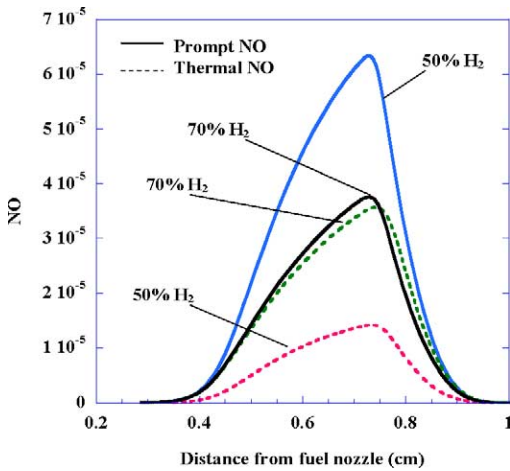


Fig. 13. Thermal and prompt NO profiles for nonpremixed flames established using two different methane/hydrogen blends containing 50 and 70% H_2 by volume.

Fig. 12a), since the adiabatic flame temperature increases with hydrogen addition. For the four cases depicted in Fig. 12, the peak flame temperatures are 2027, 2130, 2199, and 2294 K, and the corresponding adiabatic flame temperatures are 2324, 2368, 2408, and 2484 K, respectively. The flame width also increases with H_2 in the fuel blend, since the effective mass diffusivity is enhanced due to hydrogen addition. The effect of hydrogen addition on NO emission is illustrated in Fig. 12b. Although the peak NO value exhibits a nonmonotonic variation with H_2 concentration, as it first increases (for H_2 up to 50% by volume) and then decreases, the important observation is that hydrogen addition has a relatively minor effect on NOx concentration in methane flames. The peak NO varies in a very narrow range as the amount of H_2 in the blend is increased from 10 to 90% by volume. This can be attributed to the fact that the addition of H_2 decreases the prompt NO, as it lowers the CH concentration, but increases the thermal NO due to the higher flame temperature. This is confirmed by plotting the thermal and prompt NO profiles shown in Fig. 13. The prompt NO decreases while the thermal NO increases as H_2 in the blend is increased from 50 to 70% by volume. Since these two effects essentially cancel each other, the hydrogen addition has an inconsequential effect on NOx concentration in methane flames.

Fig. 14 presents the temperature and NO mole fraction profiles for nonpremixed flames established using different *n*-heptane/hydrogen fuel blends without nitrogen dilution. For the four cases depicted in the figure, the fuel blend contains 10, 50, 70, and 90% H_2 by volume or 0.22, 1.96, 4.46, and 15.25% H_2 by mass. It is important to note that for the same

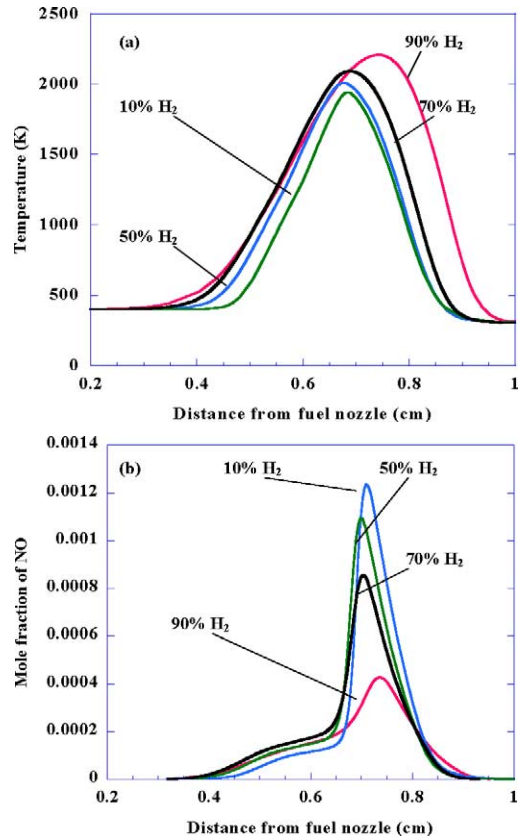


Fig. 14. Temperature (a) and NO mole fraction (b) profiles for nonpremixed flames established with different *n*-heptane/ H_2 blends at $a_s = 100 \text{ s}^{-1}$.

amount of H_2 by volume, the hydrogen mass in a *n*-heptane/hydrogen blend is much smaller than that in a methane/hydrogen blend. The temperature profiles in Fig. 14a indicate that the addition of H_2 in the fuel blend increases the flame temperature and thickness. However, the effect is small compared to that observed for CH_4 - H_2 blends.

The NO mole fraction profiles presented in Fig. 14b indicate that the NOx emission in *n*-heptane flames can be significantly reduced using H_2 addition, which is in contrast to that for methane flames, for which the NOx emission is only marginally affected by H_2 addition. For *n*-heptane flames, as the amount of H_2 in the blend is increased, it significantly lowers the NO concentration. As noted earlier, 50 and 70% H_2 by volume represent only 1.96 and 4.46% H_2 by mass, implying that a relatively small H_2 mass can significantly reduce NO emission in *n*-heptane flames. This is due to the fact that most of the NO in *n*-heptane flames is formed through the prompt mechanism, and the prompt NO is significantly reduced by adding H_2 in the blend. This is confirmed by the prompt and thermal NO profiles

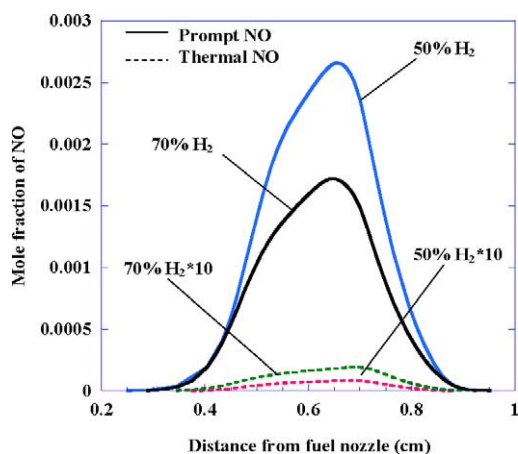


Fig. 15. Thermal and prompt NO profiles for nonpremixed flames established using two different *n*-heptane/hydrogen blends containing 50 and 70% H₂ by volume or 1.96 and 15.25% H₂ by mass.

shown in Fig. 15. As hydrogen mass in the blend is increased from 1.96 to 4.46%, the prompt NO decreases considerably while the thermal NO increases only slightly. As indicated in Fig. 15, the addition of hydrogen in the blend leads to a significant reduction in CH concentration, which causes a significant reduction in prompt NO. Although the addition of hydrogen increases thermal NO due to the increased flame temperature, its effect on the total NO is negligible, due to the dominance of the prompt mechanism. Thus an important observation here is that the addition of hydrogen can significantly reduce NO_x emission in *n*-heptane flames but has a negligible effect in methane flames.

5. Conclusions

In this numerical study we have examined the effects of using different fuels on NO_x emissions in counterflow nonpremixed and partially premixed flames. The fuels investigated include methane, *n*-heptane, and their blends using hydrogen. Methane flames have been computed using the GRI-Mech 3.0 mechanism, while *n*-heptane has been computed by combining the Held et al. oxidation mechanism with the Li and Williams NO_x mechanism. While these mechanisms have been validated previously in several configurations, two additional validations for the simulation of methane and *n*-heptane PPFs have been provided in the present study. A detailed investigation has been conducted to characterize the fuel effects on NO_x emissions. Important observations are the following:

- (1) In the context of NO_x characteristics, the partial premixed combustion can be classified into two distinct regimes, namely a double-flame regime and a merged-flame regime. In the first regime, a partially premixed flame contains two distinct or physically separated reaction zones, namely a rich premixed zone on the fuel side and a nonpremixed zone on the oxidizer side. In the second regime, these two reaction zones are nearly merged. The double-flame regime is characterized by relatively high levels of partial premixing and low strain rates. With increasing ϕ and/or a_s , the two reaction zones move closer and eventually merge, representing a transition to the merged-flame regime. Due to the difference in fuel pyrolysis/oxidation chemistry, the ranges of ϕ and a_s for the double-flame regime are significantly different for the two fuels. For counterflow methane flames, this regime is approximately given by $1.4 < \phi < 2.0$ and $20 < a_s < 50 \text{ s}^{-1}$, while for *n*-heptane flames, it is given by $1.5 < \phi < 3.5$ and $20 < a_s < 120 \text{ s}^{-1}$.
- (2) In the double-flame regime, NO_x characteristics of both methane and *n*-heptane flames are strongly affected by changes in ϕ and a_s , while in the merged-flame regime, they exhibit a relatively weak dependence on ϕ and a_s . Moreover, in the double-flame regime, the methane and *n*-heptane flames established under identical conditions exhibit widely different NO_x emission behavior, while in the merged-flame regime, their NO_x characteristics are qualitatively similar. These differences are also observed in the NO_x emission indices for both the methane and the *n*-heptane flames and are related to their respective fuel oxidation chemistry.
- (3) Under identical conditions, the amount of NO produced in *n*-heptane flames is significantly higher than that in methane flames, and this is directly attributable to the higher concentration of acetylene in *n*-heptane flames. A rate of production analysis indicated that the consumption of *n*-heptane occurs mainly through the C₂ path, while that of methane occurs mainly through the C₁ path, with the implication that the amount of C₂H₂ formed in *n*-heptane flames is significantly higher than that in methane flames. This leads to a much higher concentration of CH radicals and, consequently, of prompt NO in *n*-heptane flames. The thermal NO is also higher in *n*-heptane flames due to the higher temperature and higher O and OH radical concentrations. Consequently, the amount of total NO formed in *n*-heptane flames is significantly higher than that in methane flames.

- (4) For both methane and *n*-heptane flames, the NO level in the nonpremixed reaction zone far exceeds that in the premixed reaction zone. This is due to the paucity of O and OH radicals and to a lesser extent to lower temperature in the premixed zone. While CH radicals are produced in both the premixed and the nonpremixed reaction zones and immediately lead to the formation of HCN through the reaction $\text{CH} + \text{N}_2 \leftrightarrow \text{HCN} + \text{N}$, the subsequent conversion of HCN to NO occurs mainly in the nonpremixed zone due to the availability of O and OH radicals there. Consequently, the prompt NO is much higher in this zone than in the premixed zone. The thermal NO is also higher in the nonpremixed zone due to the higher temperature and radical concentration in this zone.
- (5) Another important difference in the NO_x characteristics of the two fuels pertains to the relative contributions of the prompt and thermal mechanisms in the two regimes. For *n*-heptane flames, the prompt mechanism is the major contributor to the total NO in both the double-flame and the merged-flame regimes. In contrast, for methane flames, the thermal mechanism is the major contributor to the total NO in the double-flame regime, while the prompt mechanism becomes the major contributor in the merged-flame regime. This switch between the relative contributions of the thermal and prompt NO during transition from the double-flame to the merged-flame regime occurs only in methane flames. It is also noteworthy that for *n*-heptane flames, the amount of NO formed due to the prompt mechanism far exceeds that formed due to the thermal mechanism in the entire partially premixed regime, and the difference becomes greater with increase in ϕ and a_s . This is again attributable to the significantly higher amount of acetylene produced in the premixed zone, which is subsequently transported to the nonpremixed zone in *n*-heptane flames. In contrast, for methane flames, the amount of acetylene transported to the nonpremixed zone is relatively small, and the relative contributions of the prompt and thermal mechanisms are generally comparable.
- (6) NO_x characteristics of methane/hydrogen and *n*-heptane/hydrogen blends have also been investigated. Results indicate that the addition of hydrogen can significantly reduce NO_x emission in *n*-heptane flames but has a negligible effect on NO_x emission in methane flames. This is due to the fact that most of the NO in *n*-heptane flames is produced through the prompt mechanism, and the prompt NO is significantly reduced by H₂, since the C₂H₂ and, consequently, the CH con-

centrations are reduced due to H₂ addition. In contrast, for methane flames, the decrease in the prompt NO due to hydrogen addition is balanced by the corresponding increase in the thermal NO, and the total NO is essentially unaffected by hydrogen addition.

Acknowledgments

This research was supported by the NSF Combustions and Plasma Systems Program for which Drs. Farley Fisher and Thomas Chapman have been the Program Directors. We thank Professor F.L. Dryer and Dr. T. Held for providing the *n*-heptane mechanism, Mr. Hongshe Xue for help with numerical simulations, and Mr. Paolo Berta for performing *n*-heptane flame simulations using a more comprehensive mechanism. Many stimulating discussions with Professor I.K. Puri are gratefully appreciated.

References

- [1] R.S. Barlow, C.D. Carter, *Combust. Flame* 104 (1996) 288–299.
- [2] A.N. Hayhurst, A.D. Lawrence, *Combust. Flame* 105 (1996) 341–357.
- [3] M.C. Meunier, M.G. Carvalho, *Combust. Flame* 112 (1998) 221–230.
- [4] A. Schlegel, P. Benz, T. Griffin, W. Weisenstein, H. Bockhorn, *Combust. Flame* 105 (1996) 332–340.
- [5] C. Poppe, S. Sivasegaram, J.H. Whitelaw, *Combust. Flame* 113 (1998) 13–26.
- [6] S.C. Li, F.A. Williams, *Combust. Flame* 118 (1999) 399–414.
- [7] J. Warnatz, P. Klaus, CEC reaction mechanism for methane/air combustion, <http://www.ca.sandia.gov/tdf/3rdworkshop/chemmech/JW-C2NO98.mec.html>.
- [8] Leeds NO_x mechanism, <http://www.chem.leeds.ac.uk/combustion/nox.html>.
- [9] J.A. Miller, C.T. Bowman, *Prog. Energy Combust. Sci.* 15 (1989) 287.
- [10] C.E. Roberts, Determination of the effect of water on soot formation, <http://www.swri.edu/3pubs/IRD1999/03907399.htm>.
- [11] G.J. Rortveit, J.E. Hustad, S.C. Li, F.A. Williams, *Combust. Flame* 130 (2002) 48–61.
- [12] D. Zhao, H. Yamashita, K. Kitawaga, N. Arai, T. Furuhata, *Combust. Flame* 130 (2002) 352–360.
- [13] G.J. Rortveit, J.E. Hustad, F.A. Williams, NO_x formation in diluted CH₄/H₂ counterflow diffusion flames, in: *Proc. of the 6th International Conference on Technologies and Combustion for a Clean Environment*, Porto, Portugal.
- [14] M.A.S. Al-Baghdadi, *Renewable Energy* 28 (9) (2002) 1471–1478.
- [15] A.R. Choudhuri, S.R. Gollahali, *Int. J. Hydrogen Energy* 28 (4) (2002) 445–454.

- [16] J.P. Gore, N.J. Zhan, *Combust. Flame* 105 (1996) 414–427.
- [17] M.A. Tanoff, M.D. Smooke, R.J. Osborne, T.M. Brown, R.W. Pitz, *Proc. Combust. Inst.* 26 (1996) 1121–1128.
- [18] R.V. Ravikrishna, N.M. Laurendeau, *Combust. Flame* 122 (2000) 471–482.
- [19] R.S. Barlow, A.N. Karpets, J.H. Frank, J.Y. Chen, *Combust. Flame* 127 (2001) 2102–2118.
- [20] V. Dupont, A. Williams, *Combust. Flame* 114 (1998) 103–118.
- [21] H.S. Xue, S.K. Aggarwal, *Combust. Flame* 132 (2003) 723–741.
- [22] H.S. Xue, S.K. Aggarwal, R.J. Osborne, T.M. Brown, R.W. Pitz, *AIAA J.* 40 (6) (2002) 1236–1238.
- [23] L.G. Blevins, J.P. Gore, *Combust. Flame* 116 (1999) 546–566.
- [24] A.E. Lutz, R.J. Kee, J.F. Grear, F.M. Rupley, OPPDIF: A Fortran program for computing opposed flow diffusion flames, Sandia National Laboratories Report No. SAND96-8243.
- [25] R.J. Kee, F.M. Rupley, J.A. Miller, Chemkin: A Fortran chemical kinetics package for the analysis of gas phase chemical kinetics, Sandia National Laboratories Report No. 89-8009B.
- [26] T.J. Held, A.J. Marchese, F.L. Dryer, *Combust. Sci. Technol.* 123 (1997) 107–146.
- [27] G.P. Smith, D.M. Golden, M. Frenklach, N.W. Moriarty, B. Eiteneer, M. Goldenberg, C.T. Bowman, R.K. Hanson, S. Song, W.C. Gardiner Jr., V.V. Lissianski, Z. Qin, GRI Mech-3.0, <http://www.me.berkeley.edu/grimech/>.
- [28] C.J. Sung, C.K. Law, J.Y. Chen, *Proc. Combust. Inst.* 27 (1998) 295–304.
- [29] C.J. Montgomery, M.A. Cremer, M.P. Heap, J.Y. Chen, C.K. Westbrook, L.Q. Maurice, Reduced chemical kinetic mechanisms for hydrocarbon fuels, in: 35th AIAA/ASME/SAE/ASEE Joint Propulsion Conference and Exhibit, Los Angeles, California, 1999.
- [30] S.G. Davis, C.K. Law, *Proc. Combust. Inst.* 27 (1998) 521–527.
- [31] R. Seiser, L. Truett, D. Trees, K. Seshadri, *Proc. Combust. Inst.* 27 (1998) 649–657.
- [32] E. Ranzi, M. Dente, G. Bozanno, A. Goldaniga, T. Faravelli, *Prog. Energy Combust. Sci.* 27 (2001) 99–139.
- [33] H. Xue, S.K. Aggarwal, *AIAA J.* 39 (2001) 637–648.
- [34] S.C. Li, F.A. Williams, *Proc. Combust. Inst.* 28 (2000) 1031.
- [35] Material Safety Data Sheet (MSDS) for methane (CH₄), Voltaix, Inc., Post Office Box 5357, North Branch, NJ 08876-5357, USA, 1994 (Revised 1996).
- [36] Material Safety Data Sheet (MSDS) for heptane, Matheson Tri-Gas, Inc., 959 Route 46 East Chemtrec 1-800-424-9300, Parsippany, NJ 07054-0624, USA, 1989 (Revised 2002).
- [37] D.C. Horning, D.F. Davidson, R.K. Hanson, *J. Propul. Power* 18 (2) (2002) 363–371.
- [38] Y. Hidaka, K. Sato, Y. Henmi, H. Tanaka, K. Inami, *Combust. Flame* 118 (1999) 340–358.
- [39] T. Turanyi, Kinalc homepage, <http://www.chem.leeds.ac.uk/Combustion/kinalc.html>.
- [40] M. Nishioka, S. Nakagawa, Y. Ishikawa, T. Takeno, *Combust. Flame* 98 (1994) 127–138.